

---

# METAMEDSEG: VOLUMETRIC META-LEARNING FOR FEW-SHOT ORGAN SEGMENTATION

---

**Anastasia Makarevich\***  
 Technical University of Munich  
 Munich, Germany  
 ana.makarevich@tum.de

**Azade Farshad\***  
 Technical University of Munich  
 Munich, Germany  
 azade.farshad@tum.de

**Vasileios Belagiannis**  
 Ulm University  
 Ulm, Germany  
 vasileios.belagiannis@uni-ulm.de

**Nassir Navab**  
 Technical University of Munich  
 Munich, Germany  
 nassir.navab@tum.de

## ABSTRACT

The lack of sufficient annotated image data is a common issue in medical image segmentation. For some organs and densities, the annotation may be scarce, leading to poor model training convergence, while other organs have plenty of annotated data. In this work, we present MetaMedSeg, a gradient-based meta-learning algorithm that redefines the meta-learning task for the volumetric medical data with the goal to capture the variety between the slices. We also explore different weighting schemes for gradients aggregation, arguing that different tasks might have different complexity, and hence, contribute differently to the initialization. We propose an importance-aware weighting scheme to train our model. In the experiments, we present an evaluation of the medical decathlon dataset by extracting 2D slices from CT and MRI volumes of different organs and performing semantic segmentation. The results show that our proposed volumetric task definition leads to up to 30% improvement in terms of IoU compared to related baselines. The proposed update rule is also shown to improve the performance for complex scenarios where the data distribution of the target organ is very different from the source organs.

## 1 Introduction

Segmentation of medical images is an effective way to assist medical professionals in their diagnosis. Recent advances in deep learning have made it possible to achieve high accuracy in organ and tumour segmentation [1, 2]. Despite the recent advances in medical image segmentation, standard supervised learning settings usually require a large amount of labelled data. Labelled data can be abundantly available for some organs (e.g., liver), yet it can be really scarce for others. One of the early approaches to overcome this limitation is transfer learning, where a neural network is pretrained on a large labelled dataset (source domain) and then fine-tuned on a small amount of labelled data (target domain) [3].

Another common approach, that gained a lot of popularity, is few-shot learning which aims to learn from just a few examples. One recent example of few-shot learning is COVID-19 detection using chest X-rays [4]. Few-shot methods can be roughly divided into augmentation-based learning and task-based meta-learning. In this work we focus on the meta-learning approach, which also comes in different flavours: metric learning (e.g., prototypical networks [5–7]), memory-based learning [8, 9] and gradient-based methods. Few-shot learning for image segmentation has been an active research topic [10–16], but there are few works [17–19] focusing on few-shot medical image segmentation.

---

\*The first two authors contributed equally to this work.  
 Project page: <http://metamedseg.github.io/>

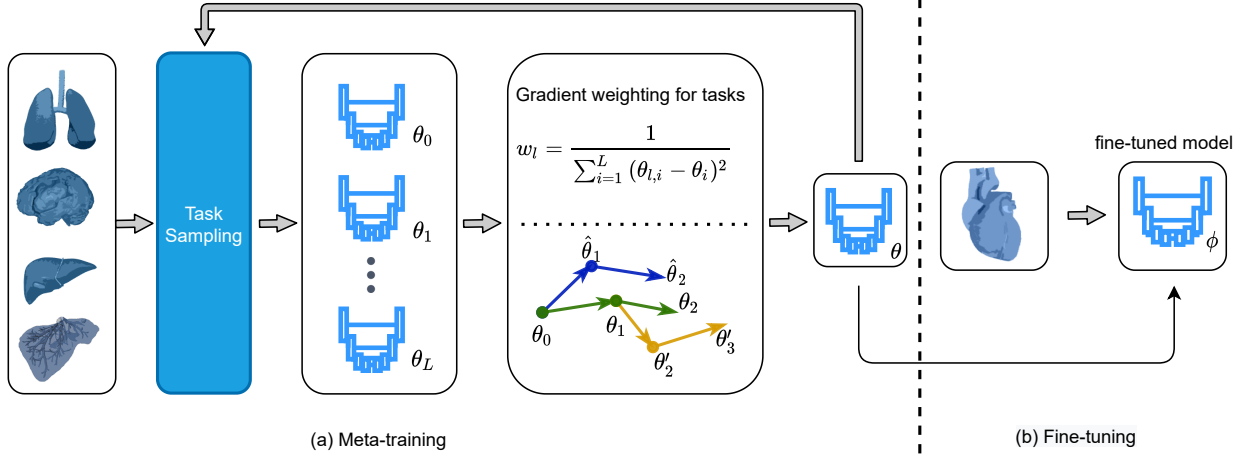


Figure 1: The meta-training step on source organs is shown on the left, where we define the meta-training tasks and weight these tasks based on their importance.  $\theta$  is the meta-model parameters and  $\phi'$  is the model in the progress of meta-training. The meta-trained model with parameters  $\phi$  is then used for the final fine-tuning step on the target organ.

In this work, we follow the meta-learning approach, relying on one of the recent modifications of the MAML (Model-Agnostic Meta-Learning) algorithm [20] - Reptile [21], which is a simple and yet effective algorithm that provides a wide field for experiments. We address the two main components of gradient-based meta-learning: task definition and gradient aggregation. By gradient aggregation, we mean the update of the weights of the meta-model. The task definition is the concept of creating tasks by sampling pairs of images and their corresponding segmentation maps based on the specified criteria. We propose a volume-based task definition, specifically designed for volumetric data, and introduce a weighting mechanism for aggregation of gradients in each meta-training step, beneficial to non-IID (independent and identically distributed) data.

The main contribution of this work is the volumetric task definition. We show that sampling data from one volume per task could lead to better optimization of the local models on the specific organ due to more control over the shots variability. In contrast to the standard setting, where tasks are sampled randomly and can as well end up with images from similar parts of the volume (e.g. just first slices of different volumes), we ensure that a certain level of diversity exists between the shots, but at the same time, the diversity of the source set in general is reduced, since each volume is associated with a fixed, limited number of shots (e.g. 15) and other shots never participate in the training, which has shown to have a positive effect on training as shown in [22]. Our second contribution is the importance-aware weighting scheme. In the classical Reptile setting, gradients of sampled tasks are averaged in each meta-epoch, while in our proposed method, the gradients are weighted based on the importance of each task. The importance is defined as the distance between a local model trained on a given task and the average of all models trained on other tasks. This weighting mechanism has been proposed before in the federated learning framework [23] for non-IID data. We argue that by giving less weight to tasks with a higher distance from the average model, less chance is given to the outlier data which could help avoid catastrophic forgetting (the tendency of the neural network to forget previously learnt information) [24]. This could also perform as a regularization to avoid overfitting when tasks are similar and benefit the training when the cross-domain distance is high.

Our evaluations show that the proposed volumetric task definition and weighted gradient aggregation improve the segmentation’s accuracy. We evaluate our method in two different settings: 1. Few-shot, where the models are fine-tuned on few shots. 2. Full-data, where the model is fine-tuned on all of the data for the target organ. We compare our results with multiple baselines: 1. Supervised learning with random initialization, 2. Supervised learning with transfer learning initialization, 3. Reptile baseline, with and without our proposed volumetric task definition, 4. Few-shot cell segmentation by Dawoud et al. [18], which is the closest related work, with and without our proposed volumetric task definition. Figure 1 shows an overview of our method.

To summarize, we propose MetaMedSeg, a meta-learning approach for medical image segmentation. The main contributions of this work are as follows: 1. A novel task definition based on data volumes designed for medical scenarios 2. A novel update rule for few-shot learning where the cross-domain distance is high. 3. Significant improvement of segmentation performance compared to standard methods.

## 2 Methodology

Given a dataset  $\mathcal{D} = \{\mathcal{S}, \mathcal{T}\}$ , we define  $\mathcal{S} = \{\mathcal{S}_1 \cdots \mathcal{S}_n\}$  as the training set (source domain) and  $\mathcal{T} = \{\mathcal{T}_1 \cdots \mathcal{T}_m\}$  as the test set (target domain), where  $n, m$  are the number of organ datasets for the source and target domains and  $\mathcal{T} \cap \mathcal{S} = \emptyset$ . Each dataset consists of pairs of images and segmentation masks. The task in our setup is defined then as a subset of  $k$  shots sampled from  $\mathcal{S}_i$  or  $\mathcal{T}_j$ .

The learning has two steps: meta-training and fine-tuning. The model parameters from the meta-training step are denoted by  $\theta$ , while the fine-tuned model parameters are denoted by  $\phi$ . At each meta-train step, each task learns its own set of parameters denoted as  $\theta_l$ , starting with meta-model weights  $\theta$ . The network architecture used in this work is the well-known U-Net [1] architecture, which is commonly used for medical image segmentation. The input to the network is a batch of images  $\mathcal{I}_b$ , the outputs are segmentation maps  $y_b$ . The ground-truth segmentation maps are denoted by  $y'_b$ . Instead of batch normalization, we adopt the instance normalization approach [25, 26] for the meta-learning setting. Algorithm 1 shows the base version of the algorithm for our approach. The main components of our work are: 1. *Meta-learning* 2. *Image Segmentation*. We discuss each of them below.

---

**Algorithm 1:** MetaMedSeg for organ segmentation

---

**Input:** Meta-train datasets  $\mathcal{S} = \mathcal{S}_1, \mathcal{S}_2, \dots, \mathcal{S}_n$

**Input:** Meta-test dataset  $\mathcal{T}$

```

1 Initialize:  $\theta$ 
2 for meta-epoch = 1, 2, ..., N do
3   Sample L datasets from meta-train datasets  $\mathcal{S}$ 
4   for  $l = 1, 2, \dots, L$  do
5     Sample K shots from dataset  $\mathcal{S}_l$  using rule  $\mathcal{R}$ 
6     Train base learner (U-Net) to obtain  $\theta_l = g(L(\theta, \mathcal{S}_l))$ 
7   Compute task importance  $w_l$ 
8   Perform meta-update:  $\theta \leftarrow \theta + \beta \sum_{l=1}^L w_l(\theta_l - \theta)$ 
9 Sample  $K'$  shots from meta-test dataset  $\mathcal{T}$  to generate  $T' \in \mathcal{T}$ 
10 Fine-tune on  $T'$ 
11 Compute test IoU on  $T'' \in \mathcal{T}, T' \cap T'' = \emptyset$ 

```

---

### 2.1 Meta-learning

As shown in fig. 1, in each round of meta-training, a set of tasks consisting of images and their corresponding segmentation maps are sampled according to the chosen rule and fed to the U-Net model. The learned weights of all of these models are then aggregated based on the specified update rule. The final model is used as initialization for the fine-tuning step. In classical Reptile algorithm [21], the updates obtained from all tasks are averaged in each meta-epoch. We propose a different strategy for weighting these updates based on the importance of the tasks. The details of task definition, task sampling and update rules will be discussed next.

#### 2.1.1 Task definition

A task in meta-learning for segmentation can be defined in different ways. Our initial approach is based on [18]. A task is a set of  $k$  images and masks belonging to the same dataset. For example,  $k$ -shots sampled randomly from all available vessel cancer slices is such a task. This approach is targeted mainly at 2D data, and although we are also working with 2D slices, there is additional information that could be used. Our data is not just a set of images but a set of volumes (3D tensors that can be sliced along chosen direction to produce sets of 2D images), so we propose a volume-based task definition. We suggest defining a task as a set of images from the same volume  $\mathcal{V}$  sampled with the step size =  $\left\lceil \frac{|\mathcal{V}|}{K} \right\rceil$ . This ensures the balancedness of task sizes across datasets.

#### 2.1.2 Weighted task sampling

Some organs have different modalities and/or different zones (e.g. prostate can be split into peripheral and transitional zones), which we treat as separate datasets. One can see that this might lead to some organs dominating during task sampling (e.g. BRATS dataset alone is translated into 12 different source datasets). To counter that, we suggest using weighted sampling to give each organ a fair chance to get into the tasks set in each meta-epoch. For each organ with  $z$  different modalities or zones, we set the sampling rate of each modality / zone to  $\frac{1}{z}$  and normalize them.

### 2.1.3 Importance-aware task weighting

We employ the original Reptile [21] update rule as a baseline for our method:

$$\theta \leftarrow \theta + \beta \frac{1}{L} \sum_{l=1}^L (\theta_l - \theta), \quad (1)$$

where  $\theta_l$  is the weights vector of the local model,  $\theta$  is the weights vector of the meta-model,  $L$  is the number of tasks and  $\beta$  is the meta learning rate. We compare the following settings:

- Average weighting (AW): all updates have the same weights and  $(\theta_l - \theta)$  are averaged across tasks.
- Inverse distance weighting (IDW): more weight is given to models closer to the meta-model.

The weights for AW update are defined by the number of tasks sampled in each meta-epoch. With  $L$  tasks sampled, the weights for each of tasks would be:  $\frac{1}{L}$ . The weighting for the inverse distance update is given by:

$$w_l = \frac{1}{\sum_{i=1}^L (\theta_{l,i} - \theta_i)^2}, \quad (2)$$

where  $\theta_i$  is the  $i$ -th weight of the meta-model and  $w_{l,i}$  is the  $i$ -th weight of the  $l$ -th task's model of the current meta-epoch. The weights are also normalized to sum up to 1 using  $w_l = \frac{w_l}{\sum_j w_j}$ . The update rule is therefore:

$$\theta \leftarrow \theta + \beta \sum_{l=1}^L w_l (\theta_l - \theta), \quad (3)$$

## 2.2 Image Segmentation

Binary cross entropy (BCE) is the common loss term for optimizing image segmentation models. However, our initial experiments demonstrated quite poor performance in a few-shot setting, so we experimented with other losses. We employ the weighted BCE loss in combination with the approximation of Intersection over Union (IoU) loss [27] for segmentation.

### 2.2.1 Weighted BCE Loss

Given an input image  $\mathcal{I}$ , predicted segmentation map  $y$  and ground truth segmentation map  $y'$ , the weighted BCE loss is calculated as:

$$BCE(y, y') = -(p_{\text{pos}} y \log(y') + (1 - y) \log(1 - y')) \quad (4)$$

where  $p_{\text{pos}}$  is the weight of positive samples (ratio of sum of object pixels to sum of background pixels).

### 2.2.2 IoU loss

For the IoU loss, we adopt the IoU approximation proposed by Rahman et al. in [27], defined as:

$$\begin{aligned} \mathcal{X}(y, y') &= \sum_{i \in \mathcal{P}} y_i * y'_i \\ \mathcal{U}(y, y') &= \sum_{i \in \mathcal{P}} (y_i + y'_i - y_i * y'_i) \\ IoU(y, y') &= \frac{\mathcal{X} + \epsilon}{\mathcal{U} + \epsilon}, \end{aligned} \quad (5)$$

where  $\mathcal{P}$  is the set of all training images pixels,  $y_i$  is the ground truth pixel value (0 for background, 1 for object), and  $y'_i$  is the probability - the sigmoid output of the U-Net. We add  $\epsilon$  to the formula for numerical stability. Finally, we experiment with the combination of BCE and logarithmic DICE loss, using Equation 6 (see derivation in the supplementary material):

$$Q(L(y, y')) = BCE(y, y') - \log \left( \frac{2IoU(y, y')}{IoU(y, y') + 1} \right) \quad (6)$$

Table 1: Comparison of our proposed methods to related work in a few-shot setting, fine-tuned on 15 shots on 4 different organs. AW and IDW stand for Average weighting and Inverse distance weighting respectively.

Update rule	Target organ	IoU $\uparrow$	
		Standard	Volume-based
Supervised Learning	Cardiac	58.78	—
Transfer Learning	Cardiac	66.22	—
Dawoud et al. [18]	Cardiac	68.28	67.7
MetaMedSeg + IDW (Ours)	Cardiac	67.49	64.86
MetaMedSeg + AW (Ours)	Cardiac	67.83	<b>68.33</b>
Supervised Learning	Spleen	38.81	—
Transfer Learning	Spleen	51.18	—
Dawoud et al. [18]	Spleen	49.29	<b>58.34</b>
MetaMedSeg + IDW (Ours)	Spleen	55.64	50.50
MetaMedSeg + AW (Ours)	Spleen	55.98	56.44
Supervised Learning	Prostate Peripheral	7.35	—
Transfer Learning	Prostate Peripheral	10.87	—
Dawoud et al. [18]	Prostate Peripheral	15.99	12.82
MetaMedSeg + IDW (Ours)	Prostate Peripheral	17.15	13.89
MetaMedSeg + AW (Ours)	Prostate Peripheral	16.17	<b>22.69</b>
Supervised Learning	Prostate Transitional	38.64	—
Transfer Learning	Prostate Transitional	41.09	—
Dawoud et al. [18]	Prostate Transitional	42.85	46.28
MetaMedSeg + IDW (Ours)	Prostate Transitional	44.25	44.72
MetaMedSeg + AW (Ours)	Prostate Transitional	42.43	<b>48.33</b>

Table 2: Comparison of our proposed methods to related work in full-data setting on 4 different organs. AW and IDW stand for Average weighting and Inverse distance weighting respectively.

Update rule	Target organ	IoU $\uparrow$	
		Standard	Volume-based
Supervised Learning	Cardiac	90.26	—
Transfer Learning	Cardiac	90.46	—
Dawoud et al. [18]	Cardiac	90.38	92.47
MetaMedSeg + IDW (Ours)	Cardiac	91.38	94.51
MetaMedSeg + AW (Ours)	Cardiac	91.08	<b>95.55</b>
Supervised Learning	Spleen	86.74	—
Transfer Learning	Spleen	86.10	—
Dawoud et al. [18]	Spleen	89.65	87.53
MetaMedSeg + IDW (Ours)	Spleen	89.96	91.53
MetaMedSeg + AW (Ours)	Spleen	90.00	<b>92.27</b>
Supervised Learning	Prostate Peripheral	39.06	—
Transfer Learning	Prostate Peripheral	39.94	—
Dawoud et al. [18]	Prostate Peripheral	37.05	41.58
MetaMedSeg + IDW (Ours)	Prostate Peripheral	47.58	68.26
MetaMedSeg + AW (Ours)	Prostate Peripheral	46.20	<b>70.90</b>
Supervised Learning	Prostate Transitional	68.04	—
Transfer Learning	Prostate Transitional	69.84	—
Dawoud et al. [18]	Prostate Transitional	70.42	71.55
MetaMedSeg + IDW (Ours)	Prostate Transitional	68.98	<b>79.95</b>
MetaMedSeg + AW (Ours)	Prostate Transitional	67.68	78.84

### 3 Experiments

We train and evaluate our approach on the medical decathlon dataset [28], which consists of 3D MRI and CT volumes of 9 organs, namely Brain (368 volumes), Hippocampus (260), Lung (25), Prostate (32), Cardiac (20), Pancreas (279), Colon (121), Hepatic Vessels (216), and Spleen (41). We use the U-Net [1] architecture and train our model using IoU, BCE, and the combination of the two losses.

As a baseline, we implement the transfer learning approach, where we train with all available training data to obtain the initialization weights for fine-tuning.

To make sure that the results obtained in the experiments are not due to the specific k-shot selection we perform fine-tuning on 5 different random selections and test on the same test set of previously unseen data. The evaluation metric (IoU) is then averaged over the 5 runs.

#### 3.1 Experimental Setup

The data is pre-processed by splitting different techniques (e.g. T2 and FLAIR) and different regions (e.g. edema and tumour) into separate datasets, which results in 24 different datasets. For each dataset, we set a threshold indicating whether we consider an object present on the image or not based on the number of pixels and visual inspection of the results. The values of thresholds can be found in the supplementary material. All the images were resized to  $256 \times 256$  resolution. The threshold was applied after resizing. We also apply volume normalization during slicing by subtracting the mean and dividing by the standard deviation of all the non-zero pixels of the whole volume. We fix the same conditions for all fine-tuning experiments: we train for 20 epochs using weight decay  $3 \times 10^{-5}$ , learning rate  $\alpha = 0.005$  with a step learning rate decay of  $\gamma = 0.7$  at every other step. For full-data training, we use a learning rate 0.001 and weight decay  $w = 3 \times 10^{-5}$ . For meta-training we train for 100 epochs, sampling 5 tasks with 15 shots and 1 image per shot at each meta-epoch. We used a learning rate of  $\alpha = 0.01$  for local and meta-model with weight decay of  $w = 0.003$  and the same learning rate decay described above. For transfer learning, we train on all datasets excluding cardiac, prostate, and spleen for 20 epochs.

To compare with [18], we use the same hyperparameters as in the original paper for meta-training. It should be noted that, following the protocol from [18], we go sequentially over all the available source datasets rather than sampling them. Also, following the same protocol, for each task, we sample 2 additional tasks for 2 additional losses from different source datasets. For fine-tuning we also follow [18], but train for 40 epochs instead of 20 to get better performance and also use IoU loss instead of BCE.

#### 3.2 Comparison to Related Work

Table 1 shows the comparison of our work to the baseline methods in few-shot setting for 15 shots on four different organs. The performance of the models fine-tuned on the whole support set is shown in table 2. Some of examples of segmentation results are shown in fig. 2.

#### 3.3 Discussion

The results of our experiments show that volume-based task design has the most effect on the segmentation performance, especially in the full-data setting. The effect of our proposed update rule is minimal in some cases, but visible in other organs such as Prostate Transitional. This could be due to the nature of data distribution and the shapes of organs. When organ shapes have a high diversity (e.g. prostate compared to other organs), the outlier shapes could benefit from the proposed inverse distance update rule which gives less weight to gradients further from average. We hypothesize that, when using volumetric task definition, all organs have the chance to contribute to the final model in a more balanced setting. Therefore, when the weighted update rule is combined with volumetric tasks, the performance decreases. Another reason could be that the weighting of the updates helps to bias the model towards tasks that are more similar to the target. To understand the effect of image diversity, we create an adjacency matrix of the average Euclidean distances between pairs of randomly selected volumes. The results in fig. 3 show that in our target organs the following have the lowest to highest distance: cardiac, spleen, prostate. The effect of this distance is visible in the final segmentation performance of each organ.

#### 3.4 Ablation Study

We show the effect of the proposed update rule, different segmentation losses, and the volume-based task definition used in this work in table 3. The models were meta-trained using five different losses including Focal Tversky loss [29]

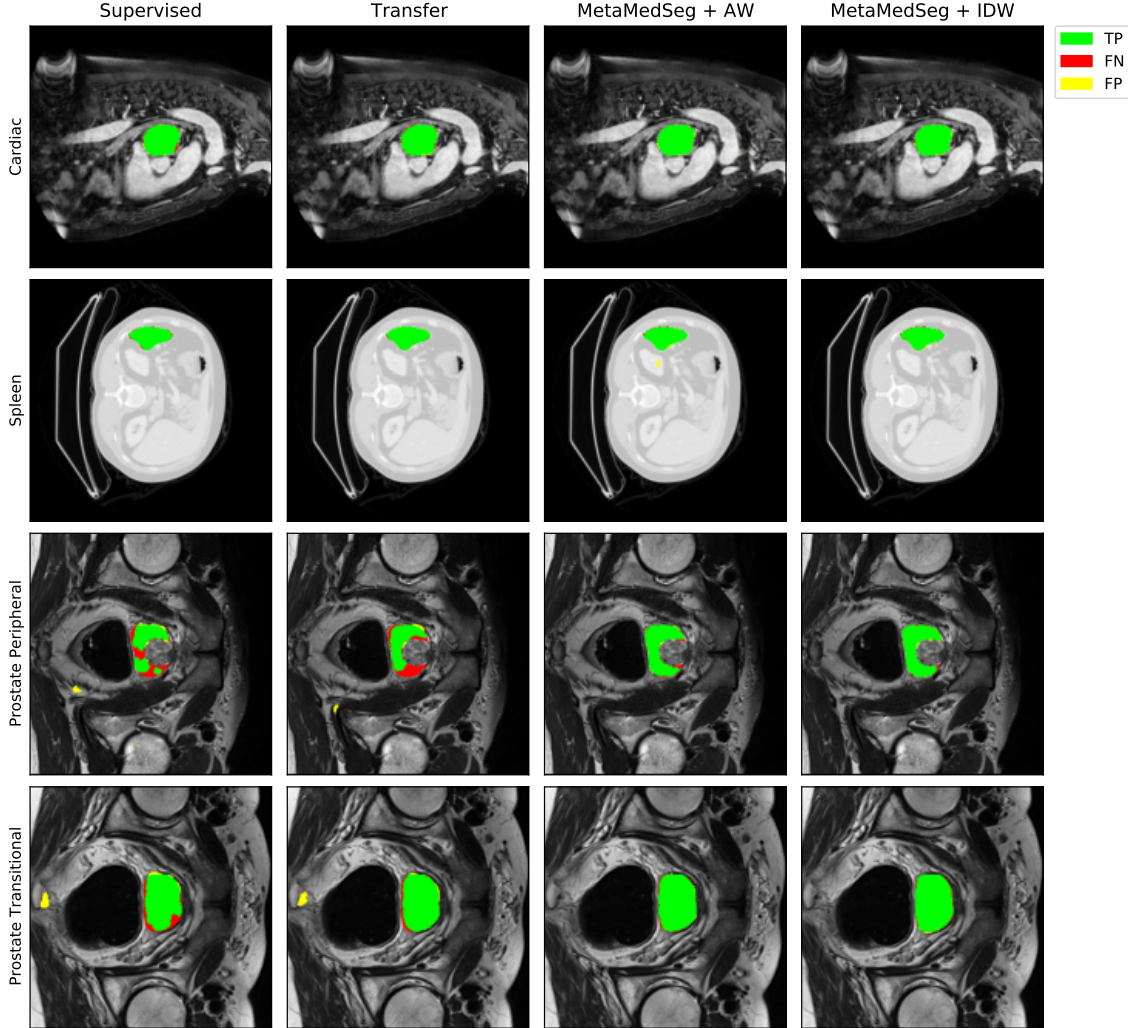


Figure 2: A comparison of different segmentation baselines with our method for four different target organs in the full-data setting.

and Dice loss [30], and then fine-tuned using IoU loss. The best performance is achieved by using weighted BCE loss for meta-training and IoU loss for fine-tuning.

## 4 Conclusion

We presented a novel way of task definition for few-shot learning for volume-based 2D data and an update rule based on the importance of tasks in the meta-training step. Our method is evaluated on four different organ types with the least amount of data, namely cardiac, spleen, prostate peripheral and prostate transitional. Our approach is not only applicable to organ segmentation but also to tumour segmentation or other types of densities. The results show that our proposed volumetric task definition improves the segmentation performance significantly in all organs. The proposed update rules provide considerable improvement in terms of IoU. Both proposed approaches (volumetric tasks and weighted update rule) could be useful in different scenarios. While the volumetric task definition proves to be advantageous in all scenarios, it is more beneficial to use the weighted update rule when the data distribution of the target class is different from the source, for example in cases such as segmentation of new diseases where also the amount of labelled data is limited.

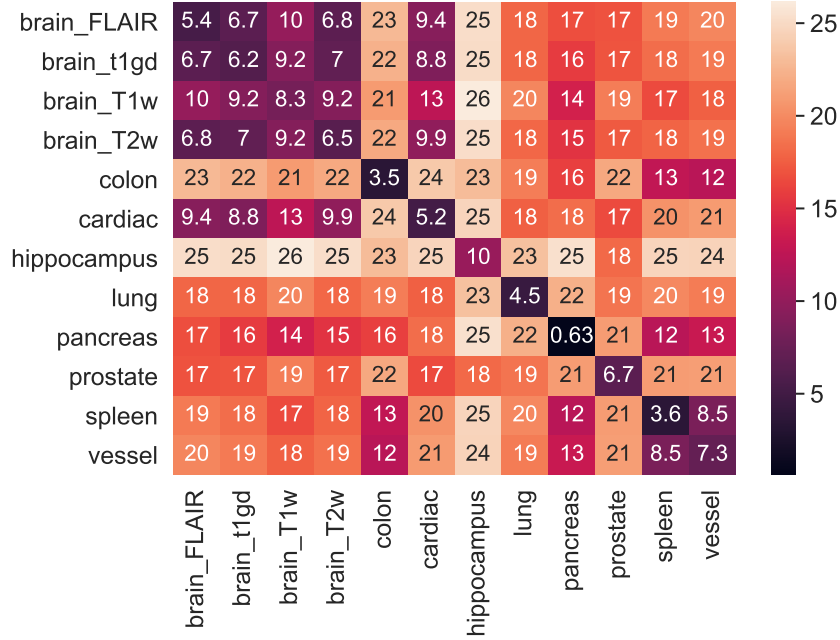


Figure 3: Heatmap of the average distances between pairs of images from different organs

Table 3: Ablation study of our method with different losses in few-shot setting for cardiac segmentation. AW and IDW stand for Average weighting and Inverse distance weighting respectively.

Update rule	Segmentation loss	IoU $\uparrow$	
		Standard	Volume-based
AW	IoU	67.82	68.13
IDW	IoU	67.42	64.86
AW	Tversky Focal loss [29]	65.90	65.72
IDW	Tversky Focal loss [29]	63.71	62.78
AW	Dice loss [30]	65.87	66.03
IDW	Dice loss [30]	62.58	62.73
AW	BCE	<b>67.83</b>	<b>68.33</b>
IDW	BCE	65.09	64.29
AW	BCE + IoU	66.85	67.30
IDW	BCE + IoU	66.98	64.71

## Acknowledgement

We gratefully acknowledge the Munich Center for Machine Learning (MCML) with funding from the Bundesministerium für Bildung und Forschung (BMBF) under the project 01IS18036B. We are also thankful to Deutsche Forschungsgemeinschaft (DFG) for supporting this research work, under project 381855581.

## References

- [1] Olaf Ronneberger, Philipp Fischer, and Thomas Brox. U-net: Convolutional networks for biomedical image segmentation. In *International Conference on Medical image computing and computer-assisted intervention*, pages 234–241. Springer, 2015.
- [2] Fausto Milletari, Nassir Navab, and Seyed-Ahmad Ahmadi. V-net: Fully convolutional neural networks for volumetric medical image segmentation. In *2016 fourth international conference on 3D vision (3DV)*, pages 565–571. IEEE, 2016.



- [3] Marcus Rohrbach, Sandra Ebert, and Bernt Schiele. Transfer learning in a transductive setting. *Advances in neural information processing systems*, 26:46–54, 2013.
- [4] Shruti Jadon. Covid-19 detection from scarce chest x-ray image data using few-shot deep learning approach. In *Medical Imaging 2021: Imaging Informatics for Healthcare, Research, and Applications*, volume 11601, page 116010X. International Society for Optics and Photonics, 2021.
- [5] Jake Snell, Kevin Swersky, and Richard Zemel. Prototypical networks for few-shot learning. In I. Guyon, U. V. Luxburg, S. Bengio, H. Wallach, R. Fergus, S. Vishwanathan, and R. Garnett, editors, *Advances in Neural Information Processing Systems*, volume 30. Curran Associates, Inc., 2017.
- [6] Kaixin Wang, Jun Hao Liew, Yingtian Zou, Daquan Zhou, and Jiashi Feng. Panet: Few-shot image semantic segmentation with prototype alignment. In *Proceedings of the IEEE/CVF International Conference on Computer Vision*, pages 9197–9206, 2019.
- [7] Boyu Yang, Chang Liu, Bohao Li, Jianbin Jiao, and Qixiang Ye. Prototype mixture models for few-shot semantic segmentation. In *European Conference on Computer Vision*, pages 763–778. Springer, 2020.
- [8] Tao Hu, Pengwan Yang, Chiliang Zhang, Gang Yu, Yadong Mu, and Cees GM Snoek. Attention-based multi-context guiding for few-shot semantic segmentation. In *Proceedings of the AAAI conference on artificial intelligence*, volume 33, pages 8441–8448, 2019.
- [9] Haochen Wang, Xudong Zhang, Yutao Hu, Yandan Yang, Xianbin Cao, and Xiantong Zhen. Few-shot semantic segmentation with democratic attention networks. In *Computer Vision—ECCV 2020: 16th European Conference, Glasgow, UK, August 23–28, 2020, Proceedings, Part XIII 16*, pages 730–746. Springer, 2020.
- [10] Zhuotao Tian, Hengshuang Zhao, Michelle Shu, Zhicheng Yang, Ruiyu Li, and Jiaya Jia. Prior guided feature enrichment network for few-shot segmentation. *IEEE Annals of the History of Computing*, pages 1–1, 2020.
- [11] Malik Boudiaf, Hoel Kervadec, Ziko Imtiaz Masud, Pablo Piantanida, Ismail Ben Ayed, and Jose Dolz. Few-shot segmentation without meta-learning: A good transductive inference is all you need? In *Proceedings of the IEEE/CVF Conference on Computer Vision and Pattern Recognition*, pages 13979–13988, 2021.
- [12] Reza Azad, Abdur R Fayjie, Claude Kauffmann, Ismail Ben Ayed, Marco Pedersoli, and Jose Dolz. On the texture bias for few-shot cnn segmentation. In *Proceedings of the IEEE/CVF Winter Conference on Applications of Computer Vision*, pages 2674–2683, 2021.
- [13] Mennatullah Siam, Boris N Oreshkin, and Martin Jagersand. Amp: Adaptive masked proxies for few-shot segmentation. In *Proceedings of the IEEE/CVF International Conference on Computer Vision*, pages 5249–5258, 2019.
- [14] Siddhartha Gairola, Mayur Hemani, Ayush Chopra, and Balaji Krishnamurthy. Simpropnet: Improved similarity propagation for few-shot image segmentation. In Christian Bessiere, editor, *Proceedings of the Twenty-Ninth International Joint Conference on Artificial Intelligence, IJCAI 2020 [scheduled for July 2020, Yokohama, Japan, postponed due to the Corona pandemic]*, pages 573–579. ijcai.org, 2020.
- [15] Weide Liu, Chi Zhang, Guosheng Lin, and Fayao Liu. Crnet: Cross-reference networks for few-shot segmentation. In *Proceedings of the IEEE/CVF Conference on Computer Vision and Pattern Recognition*, pages 4165–4173, 2020.
- [16] Pinzhao Tian, Zhangkai Wu, Lei Qi, Lei Wang, Yinghuan Shi, and Yang Gao. Differentiable meta-learning model for few-shot semantic segmentation. In *Proceedings of the AAAI Conference on Artificial Intelligence*, volume 34, pages 12087–12094, 2020.
- [17] Arnab Kumar Mondal, Jose Dolz, and Christian Desrosiers. Few-shot 3d multi-modal medical image segmentation using generative adversarial learning. *arXiv preprint arXiv:1810.12241*, 2018.
- [18] Youssef Dawoud, Julia Hornauer, Gustavo Carneiro, and Vasileios Belagiannis. Few-shot microscopy image cell segmentation. In *Machine Learning and Knowledge Discovery in Databases. Applied Data Science and Demo Track - European Conference, ECML PKDD 2020, Ghent, Belgium, September 14-18, 2020, Proceedings, Part V*, volume 12461, pages 139–154. Springer, 2020.
- [19] Cheng Ouyang, Carlo Biffi, Chen Chen, Turkay Kart, Huaqi Qiu, and Daniel Rueckert. Self-supervision with superpixels: Training few-shot medical image segmentation without annotation. In *European Conference on Computer Vision*, pages 762–780. Springer, 2020.
- [20] Chelsea Finn, Pieter Abbeel, and Sergey Levine. Model-agnostic meta-learning for fast adaptation of deep networks. In *International Conference on Machine Learning*, pages 1126–1135. PMLR, 2017.
- [21] Alex Nichol, Joshua Achiam, and John Schulman. On first-order meta-learning algorithms. *arXiv preprint arXiv:1803.02999*, 2018.

- [22] Amrith Setlur, Oscar Li, and Virginia Smith. Is support set diversity necessary for meta-learning? *arXiv preprint arXiv:2011.14048*, 2020.
- [23] Yousef Yeganeh, Azade Farshad, Nassir Navab, and Shadi Albarqouni. Inverse distance aggregation for federated learning with non-iid data. In *Domain Adaptation and Representation Transfer, and Distributed and Collaborative Learning*, pages 150–159. Springer, 2020.
- [24] Alessia Bertugli, Stefano Vincenzi, Simone Calderara, and Andrea Passerini. Few-shot unsupervised continual learning through meta-examples. *arXiv preprint arXiv:2009.08107*, 2020.
- [25] John Bronskill, Jonathan Gordon, James Requeima, Sebastian Nowozin, and Richard Turner. Tasknorm: Rethinking batch normalization for meta-learning. In *International Conference on Machine Learning*, pages 1153–1164. PMLR, 2020.
- [26] Songhao Jia, Ding-Jie Chen, and Hwann-Tzong Chen. Instance-level meta normalization. In *Proceedings of the IEEE/CVF Conference on Computer Vision and Pattern Recognition*, pages 4865–4873, 2019.
- [27] Md Atiqur Rahman and Yang Wang. Optimizing intersection-over-union in deep neural networks for image segmentation. In *International symposium on visual computing*, pages 234–244. Springer, 2016.
- [28] Amber L Simpson, Michela Antonelli, Spyridon Bakas, Michel Bilello, Keyvan Farahani, Bram Van Ginneken, Annette Kopp-Schneider, Bennett A Landman, Geert Litjens, Bjoern Menze, et al. A large annotated medical image dataset for the development and evaluation of segmentation algorithms. *arXiv preprint arXiv:1902.09063*, 2019.
- [29] Nabila Abraham and Naimul Mefraz Khan. A novel focal tversky loss function with improved attention u-net for lesion segmentation. In *2019 IEEE 16th International Symposium on Biomedical Imaging (ISBI 2019)*, pages 683–687. IEEE, 2019.
- [30] Carole H Sudre, Wenqi Li, Tom Vercauteren, Sebastien Ourselin, and M Jorge Cardoso. Generalised dice overlap as a deep learning loss function for highly unbalanced segmentations. In *Deep learning in medical image analysis and multimodal learning for clinical decision support*, pages 240–248. Springer, 2017.